ELSEVIER

Journal of Biomechanics 34 (2001) 607–612

JOURNAL OF BIOMECHANICS

www.elsevier.com/locate/jbiomech
www.JBiomech.com

On the potentially protective role of contact constraints on saccular aneurysms

P. Seshaiyer[1], J.D. Humphrey*

Biomedical Engineering Program, 233 Zachry Engineering Center, Texas A&M University, College Station, TX 77843-3120, USA

Accepted 13 December 2000

Abstract

Most intracranial saccular aneurysms remain asymptomatic until rupture. Yet, some unruptured lesions present with various symptoms, often related to the compression of a nerve or other intracranial tissue. An obvious question, therefore, is whether or not symptomatic unruptured lesions necessarily have a greater rupture-potential than asymptomatic ones. In this paper, we show numerically that contact constraints can have a protective effect on certain lesions. Specifically, finite element analyses of stress fields in model axisymmetric lesions, with and without the presence of a rigid contacting obstacle at the fundus, reveal that with the exception of near point loads, the constraint decreases the stresses near the fundus. Given that it is well accepted that rupture occurs when wall stress exceeds wall strength, these findings suggest that the rupture-potential will be lower in at least one sub-class of constrained versus comparable unconstrained lesions. Because of the myriad of sizes, shapes, and compositions of saccular aneurysms, however, there is a need to examine this important issue further, hopefully based on an increased awareness for clinical data on lesion–tissue interactions.

Keywords: Finite element analysis; Mechanical properties; Nerve compression; Stress–strain; Aneurysm rupture

1. Introduction

Recent findings suggest that the rate of rupture of intracranial saccular aneurysms may well be even less than previously thought (Wiebers et al., 1998). Nonetheless, ruptured aneurysms remain as the leading cause of spontaneous subarachnoid hemorrhage and thereby are responsible for significant morbidity and mortality. The best way to combat this devastating sequel is, of course, via early detection and appropriate treatment. Unfortunately, most saccular aneurysms are asymptomatic prior to rupture; those unruptured lesions that present symptoms often do so by pressing on adjacent structures (Sekhar and Heros, 1981). An important question that has received little attention is whether the rupture-potential of symptomatic lesions is different from that of comparably sized asymptomatic lesions. This is obviously a very difficult question, one that is complicated by the myriad of sizes, shapes, and compositions exhibited by saccular aneurysms. Nevertheless, there is a need to begin a focused dialogue.

Symptomatic unruptured aneurysms are often associated with the compression of a nerve (Wiebers et al., 1998), which likely deforms the aneurysm. One way to model this interaction would be to solve the coupled large deformation problem for the nerve and aneurysm. It is prudent, however, to first explore more general upper and lower bound solutions — for example, the effects of an infinitely stiff (i.e., rigid) or an infinitely compliant (i.e., non-existent) contacting structure on the stress distribution in an aneurysm. The former can be modeled as a 'rigid contact constraint' on the deformation of the lesion. If the associated results reveal that the effect of this constraint is potentially detrimental, then one must consider the coupled large-deformation problem. Note, however, that a constraint can be viewed, in part, as an external reactive force that serves to balance part of the load on the lesion due to the distension pressure. If the effect of such constraints are found to be protective, therefore, then there is less motivation to consider the coupled problem, whose solution would be expected to be within the upper and lower bounds.

*Correspoding author. Tel.: +1-979-845-5558; fax: +1-979-845-4450.

E-mail address: jdh@acs.tamu.edu (J.D. Humphrey).

[1] Current address: Department of Mathematics and Statistics, Box 41042, Texas Tech University, Lubbock, TX 79409-1042, USA.

0021-9290/01/$ - see front matter
PII: S0021-9290(01)00002-1

Based on a few preliminary results, the purpose of this work was to test the hypothesis that the action of a subclass of rigid contact constraints on axisymmetric saccular aneurysms is often protective. For simplicity, a fixed planar obstacle is assumed to contact the lesion at its fundus, which thereby preserves the axisymmetry. This is clearly a special case, but one that allows us to examine the potential role of a constraint for multiple lesions defined by different neck-to-height ratios, different distributions of material properties, and constraints of different lengths.

2. Methods

Due to their negligible bending stiffness, non-complicated saccular aneurysms (i.e., without atherosclerosis, thrombus, etc.) can be modeled mechanically as membranes (Kyriacou and Humphrey, 1996). Hence, consider non-complicated axisymmetric lesions wherein material points are mapped from the original configuration (R, Z) to a deformed configuration (r, z) due to a uniform quasi-static distension pressure P (Fig. 1). Moreover, let the undeformed domain be discretized by one-dimensional (1-D) quadratic finite elements. The associated principal stress resultants are (Humphrey et al., 1992)

$$T_1 = \frac{\lambda_1}{\lambda_2}\frac{\partial w}{\partial E_1}, \quad T_2 = \frac{\lambda_2}{\lambda_1}\frac{\partial w}{\partial E_2}, \tag{1}$$

where λ_α are the principal stretches, w is a pseudostrain–energy function defined per unit undeformed area, and $E_\alpha = 0.5(\lambda_\alpha^2 - 1)$ are the principal Green strains (with $\alpha = 1$ denoting the meridional and $\alpha = 2$ denoting the circumferential direction). Stress–strain data on human aneurysms have been shown to be well described by a

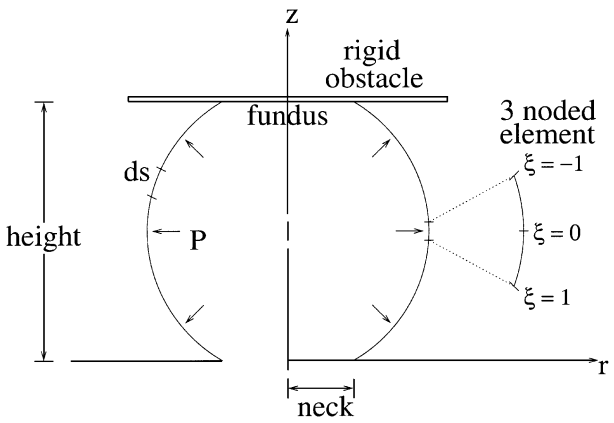

Fig. 1. Schema of an axisymmetric aneurysm constrained by a rigid planar obstacle at the fundus, with the generator curve for the undeformed geometry discretized using quadratic (three noded) elements with $\xi = (-1, 0, 1)$ at $(r, z) = (r_1, z_1, r_2, z_2, r_3, z_3)$. Also shown is the deformed arc length ds and the uniform distension pressure P.

Fung-type pseudostrain-energy function w of the form (Kyriacou and Humphrey, 1996)

$$w = c(e^Q - 1), Q = c_1E_1^2 + c_2E_2^2 + 2c_3E_1E_2, \tag{2}$$

where c is a material parameter having units of force per length and c_1, c_2, and c_3 are non-dimensional material parameters. Note: if the undeformed arc length $S \in [0, L]$, where $S = 0$ corresponds to the fundus (or pole) and $S = L$ corresponds to the neck, then $c_1 = c_2$ for all S for an isotropic behavior whereas $c_2/c_1 < 1$ (or > 1) if the material is stiffer in the meridional (or circumferential) direction at any S. Following Ryan and Humphrey (1999), we consider regional variations in material symmetries that are 'preferred', that is variations that tend to homogenize the stress distribution. This is accomplished within the finite element formulation by letting

$$\frac{c_2}{c_1} = 1 + \left[\left(\frac{c_2}{c_1}\right)_{\max} - 1\right]\left(\frac{i-1}{N-1}\right)^p, \tag{3}$$

where $(c_2/c_1)_{\max}$ is a ratio of material parameters at $S = L$, N is the total number of elements, i is the finite element number $(i = 1, \ldots, N)$, and p specifies how (e.g. linearly or non-linearly) the symmetry varies from fundus to neck. Ryan and Humphrey showed, for example, that lesions that are initally broader than tall (e.g., a large neck-to-height ratio) tend to prefer circumferential stiffening from the fundus to the neck (i.e. $(c_2/c_1)_{\max} > 1$).

There is an extensive literature on finite element analyses of finitely deformed non-linear membranes (see Jenkins and Leonard, 1991 for a review). For example, the virtual work formulation requires that

$$\int_{\Omega_0} \delta w \, \mathrm{d}A = \int_{\Omega} P\mathbf{n}.\delta\mathbf{x} \, \mathrm{d}a, \tag{4}$$

where dA and da are the original and current surface areas, respectively, $\mathbf{n}$ is an outward unit normal to da, and $\delta\mathbf{x}$ is a virtual 'displacement'. It can be shown that (4) can be written as

$$2\pi\left[\int_0^L \frac{\partial w}{\partial \mathbf{u}_e} R \, \mathrm{d}S\right]\delta\mathbf{u}_e = 2\pi\left[\int_0^L \mathrm{p}\,\boldsymbol{\psi}\frac{\mathrm{d}r}{\mathrm{d}S} r \, \mathrm{d}S - \int_0^L P\,\boldsymbol{\phi}\frac{\mathrm{d}z}{\mathrm{d}S} r \, \mathrm{d}S\right]\delta\mathbf{u}_e, \tag{5}$$

where r and z are approximated elementwise via isoparametric interpolation as, $r = \mathbf{u}_e^{\mathrm{T}}\,\boldsymbol{\phi}$ and $z = \mathbf{u}_e^{\mathrm{T}}\,\boldsymbol{\psi}$, where $\mathbf{u}_e^{\mathrm{T}} = [r_1, z_1, r_2, z_2, r_3, z_3]$ and $\boldsymbol{\phi}$ and $\boldsymbol{\psi}$ are standard quadratic shape functions. Note, too, that we enforced a zero-displacement boundary condition at the neck and a vertical-only displacement condition at the fundus, which preserves the axisymmetry.

We used a two-point Gaussian quadrature, with the Gauss points located at $\xi_1 = -\sqrt{3}/3$ and $\xi_2 = \sqrt{3}/3$ with equal weights $W_1 = W_2 = 1$, to evaluate numerically the above integrals. Due to geometric and material

non-linearities, the resulting system of algebraic equations was non-linear, and thus solved using a Newton–Raphson method. Local stress and strains were then determined at the Gauss points in postprocessing (Shah et al., 1997); the principal Cauchy stresses were computed as $t_\alpha = T_\alpha/h$, where the deformed thickness $h = H/\lambda_1\lambda_2$ from incompressibility. Convergence was shown by comparing results for 40, 100, and 400 elements.

There are several ways to model finite deformations of a membrane that is constrained by a fixed obstacle. One way is to include the contact condition in the weak form via a penalty method (Endo et al., 1984). Alternatively, Feng and Huang (1975) solve the problem by introducing a 'slack variable' and deriving an analytic expression for the total potential energy. Yet another way is to exploit the fact that when a finite element node comes into, and stays in, contact with a fixed obstacle, it loses a degree(s) of freedom. For example, instead of satisfying two separate equilibrium equations, this node would satisfy only one of the equilibrium equations along with a constraint equation for the node (Charrier et al., 1987). This is equivalent to recording the number of finite element nodes that come into contact (incrementally) with the constraint at each pressure level and then suitably modifying the boundary conditions (e.g., one can specify that the vertical displacement of a node that comes into contact with a horizontal constraint remains equal to the position of the constraint). Because we consider frictionless boundary conditions, we allow the nodes to slide along the length of the horizontal obstacle (Fig. 1). The original boundary value problem was thus solved using an updated set of boundary conditions.

Specifically, following Kyriacou and Humphrey (1996) and Shah et al. (1997), we considered an idealized sub-class of model lesions having different initial geometries (i.e., lesions with different neck-to-height ratios with the undeformed geometry being a truncated sphere or ellipse), but otherwise the same initial volume (0.0398 ml) and uniform undeformed wall thickness ($H = 27.8\,\mu m$). For isotropic behavior, we let $c_1 = c_2 = 11.82$, $c = 0.08769\,\mathrm{Nm}^{-1}$, and $c_3 = 1.18$ at all S for all geometries (from Kyriacou and Humphrey, 1996); for anisotropic (preferred) behavior, we used the values of $(c_2/c_1)_{max}$ and p found in Table 1 in Ryan and Humphrey (1999). Furthermore, we considered two different equilibrium pressures (80 and 160 mmHg) for each of the six classes of lesions (i.e., the three geometries and two distributions of material properties), and evaluated in each case the effects of seven different contact constraints as follows. First, we set the obstacle far enough away so that no part of the deformed lesion would contact it (lower bound solution). Next, we moved the obstacle to about 90% of the maximum displacement achieved by the center node of the unconstrained lesion under a distension pressure of 160 mmHg. This guarantees that at least some part of the lesion will contact the obstacle. Similarly, we then moved the obstacle to about 30% of the maximum displacement of the center node. In each case, we considered three different obstacle lengths: one greater than, one equal to 25% of, and one equal to 3.75% of the radius at the neck.

3. Results

Multiaxial stresses were decreased in all lesions due to the application of the medium and long constraints. For example, consider the case of an anisotropic lesion having an undeformed neck-to-height ratio greater than 1 (Fig. 2). This geometry can have a large radius of curvature and thus large stresses at the pole (Shah et al., 1997) and generally represents a severe case. The

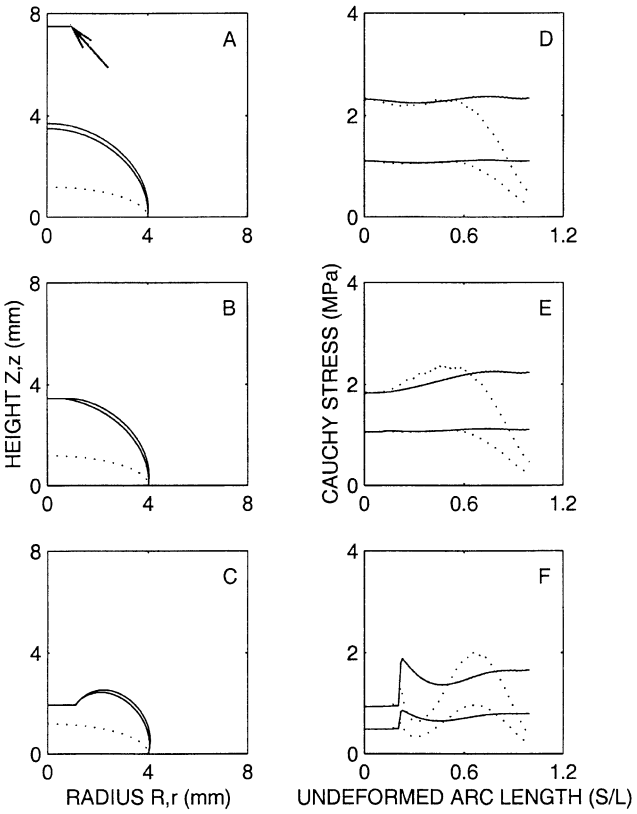

Fig. 2. Finite element simulation of an anisotropic lesion defined by a neck-to-height ratio greater than 1.0 ($\approx 4:1$) coming into contact with a 1 mm long obstacle (denoted by the ↖ in panel A). Undeformed and deformed configurations are given in panels A–C as dotted and solid curves, respectively. Associated Cauchy stresses are shown in panels D–F, respectively, in both the meridional (solid) and circumferential (dotted) directions as a function of a non-dimensional undeformed arc length S/L, with the fundus at $S = 0$. The 'pairs' of results are for $P = 80$ and 160 mmHg. Results are for the constraint placed at 90 % (panel B) and 30% (panel C) of the maximum displacement achieved by the center node in the unconstrained case. Note the protective effect of the constraint with regard to wall stress.

undeformed generator curves (dotted curves in panels A–C) reveal the prescribed geometry, one half of an ellipse. These panels also show how the initally undeformed geometry was deformed (see solid curves) under the respective distension pressure and corresponding boundary conditions (e.g., 1 mm long constraint). The results are for two distension pressures, 80 and 160 mmHg. The corresponding distributions of the principal Cauchy stresses are shown in panels D–F: meridional (solid curve) and circumferential (dotted curve). Results in panel D are the same as in Ryan and Humphrey (1999). Comparing results in panels E and F to those in D reveal that this constraint is protective, that is the multiaxial stresses were either reduced or unchanged relative to the unconstrained lesion. Note also, that the effects are localized near the obstacle. Given that lesions with preferred symmetries generally have lower stresses than geometrically comparable ones that are isotropic (Ryan and Humphrey, 1999), and because we seek upper bound solutions, we then considered isotropic lesions. Results for the same geometry, same constraint, same pressures but isotropic behavior were similar to those of Fig. 2 though with generally higher stresses (Fig. 3). Next, consider a lesion with a small neck-to-height ratio and isotropic behavior. As noted above, both the medium (0.5 mm long; not shown) and long (4 mm; Fig. 4) obstacle again reduced the stresses relative to those in the comparable unconstrained lesions. Indeed, similar results were found for lesions having equal neck-to-height ratios (not shown). Albeit perhaps physiologically unrealistic, next consider the effects of very short obstacles (3.75% of the neck), which should provide further upper bound information.

As expected, in all cases significant 'indentation' by short obstacles resulted in marked increases in the stresses near the fundus. For example, consider the case of a lesion with an equal neck-to-height ratio, short obstacle (0.1 mm long), and isotropic behavior (Fig. 5). As it can be seen in panel F, the stresses increased by more than 100% when the 'indentation' was 30% of the maximum displacement achieved by the fundus of the unconstrained lesion at 160 mmHg. This potentially detrimental effect is akin to the application a point load, hence the significant stress concentration near the symmetry axis.

4. Discussion

The primary clinical predictor of the rupture-potential of saccular aneurysms continues to be their maximum

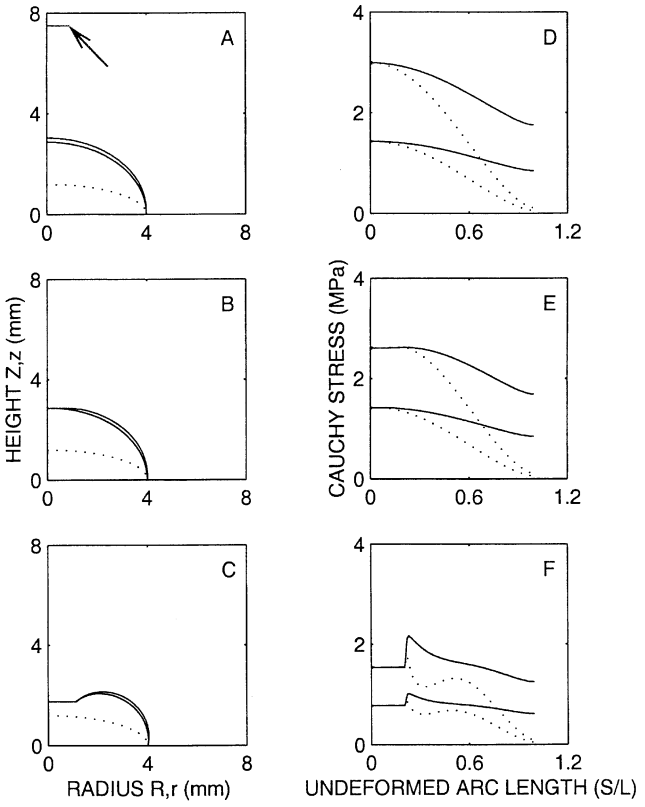

Fig. 3. Similar to Fig. 2 but for an isotropic lesion coming into contact with a medium length obstacle.

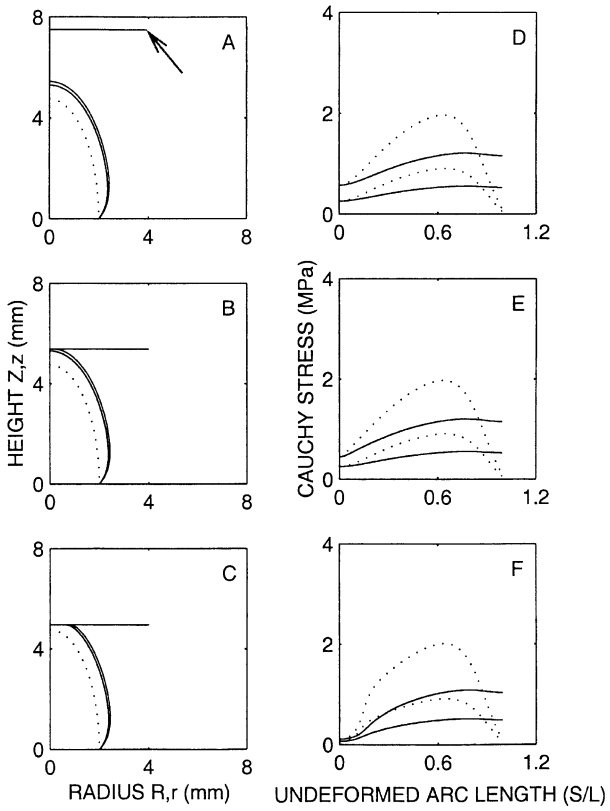

Fig. 4. Similar to Fig. 2 but for an isotropic lesion defined by a neck-to-height ratio of ≈ 0.4 subjected to a long obstacle (4 mm).

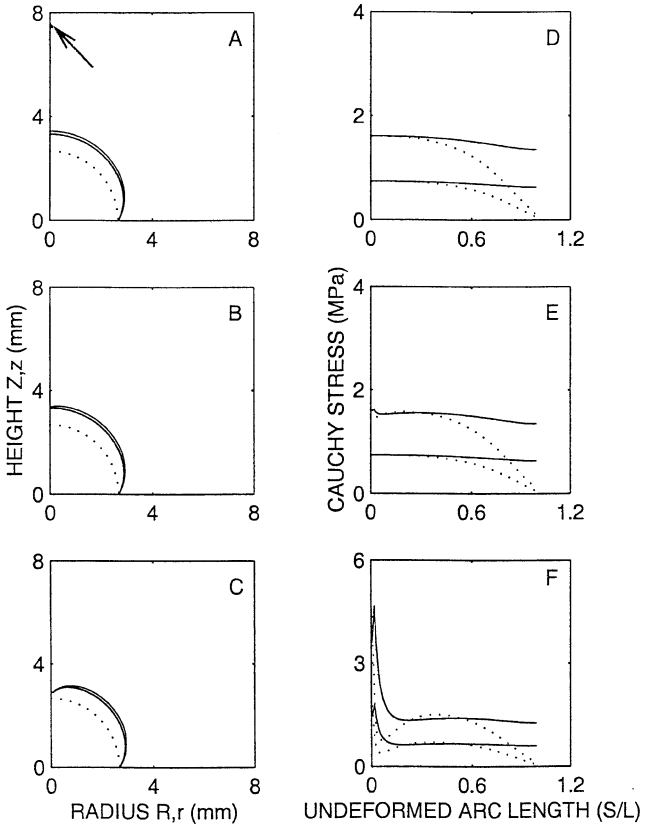

Fig. 5. Similar to Fig. 2 but for an isotropic lesion defined by a neck-to-height ratio of 1.0 subjected to a short obstacle (0.1 mm). Note the marked increase in stresses near the fundus, similar to that expected of a point load.

dimension despite significant controversy over the 'critical size' and recent work that reveals the importance of the local curvature rather than size alone (Shah et. al., 1997). Moreover, there has yet to be an analysis of additional complexities such as the presence of atherosclerotic patches, intraluminal thrombi, the effects of prior bleeds, or contact with nearby tissues, including nerves. It is well known, for example, that some patients present with cranial nerve deficits due to the pressing of an aneurysm (Wiebers et. al., 1998). We hypothesized that a simple class of contact constraints on saccular aneurysms could be protective (e.g., the contacting structure could carry some of the load acting on the aneurysm). Because every saccular aneurysm is biomechanically distinct, however, it is unreasonable to address this hypothesis with a lesion-specific analysis. Rather, we tested our hypothesis for *sub-classes* of axisymmetric lesions, defined by varying neck-to-height ratios and varying material properties, which contact a fixed planar obstacle at the fundus. Such analyses serve as a beginning to help guide retrospective and prospective statistical analyses of actual lesions, which is necessary to improve our overall understanding of the natural history of saccular aneurysms.

The finite element method is a convenient tool for performing parametric studies via numerical simulations. Such analyses have, nonetheless, appeared only recently. For example, Kyriacou and Humphrey (1996) were the first to investigate the non-linear behavior of various idealized axisymmetric models of saccular aneurysms. The present results are likewise the first to address the interaction of model aneurysms with an obstacle; it is unfortunate that there are no results in the literature to which the present ones can be compared. Despite providing some insight, we note that this study is limited. For example, we assumed that the obstacle contacts the lesion only at its fundus, hence preserving the axisymmetry. More general, and complex, non-axisymmetric cases will need to be studied. Also, we assumed a frictionless contact with a rigid obstacle whereby the inflation is constrained only in the direction normal to the constraint. On the other hand, one could consider no-slip contact conditions whereby the lesion cannot experience further displacements at the points of contact, or one could model the interaction with a non-linearly elastic obstacle. For aneurysms, however, it seems reasonable to consider a frictionless contact given the presence of abundant extravascular fluid which could serve as a mild lubricant as well as the pulsatility of the loadings which would tend to allow intermittent slipping. Certainly nerves and most other intracranial structures are deformable, but the rigid assumption is thought to provide an upper bound solution. Although what we have considered in this paper is only a special case, it does suggest a potentially protective role of contact constraints except when the obstacle acts nearly as a point load.

Specifically, our results first suggest that when a lesion comes in contact with medium or long obstacles the values of meridional and circumferential stresses actually decrease (panels E and F in Figs. 2–4) when compared to the control case (panel D of each figure). Assuming dependence of rupture-potential on the multiaxial state of stress, suggests that there is less chance of rupture due to the presence of such a constraint. Conversely, when a lesion contacts a short obstacle, it is possible that the stresses increase near the contact, which could be detrimental and could contribute to rupture (Fig. 5). Although very short constraints may be physiologically unlikely, such cases should be considered to ensure relatively complete investigation. Indeed the short constraint makes the computational problem more involved, for to specify the constraint boundary conditions, one not only needs to calculate the number of nodes that would cross the constraint as before, but also count (among these) the number of nodes whose displacement in the horizontal direction is less than the length of the constraint. This number gives the new set of boundary conditions that needs to be appended along with the old boundary conditions while solving the overall problem.

Finally, it is important to emphasize that aneurysms are not inert structures subjected to constant loads and boundary conditions. As noted in Ryan and Humphrey (1999) and Canham et al. (1999), it appears that these lesions may enlarge via a process of stress-mediated growth and remodeling. If so, the altered stress distribution due to a constraint would, in turn, affect the properties and thus the response. We did not model this process, though it merits attention. In conclusion, we emphasize that the present results strictly apply only to specific types of contact and for idealized axisymmetric aneurysms. Nonetheless, in most cases studied, the rupture-potential of the 'symptomatic lesions' would likely be less than that of comparable asymptomatic ones. There is a need, therefore, to consider contact constraints in interventional decisions.

Acknowledgements

This work was supported by a grant from the National Institutes of Health (HL 54957).

References

Canham, P.B., Finlay, H.M., Kiernan, J.A., Ferguson, G.G., 1999. Layered structure of saccular aneurysms assessed by collagen birefringence. Neurology Research 21, 618–626.

Charrier, J.M., Shrivastava, S., Wu, R., 1987. Free and constrained inflation of elastic membranes in relation to thermoforming-axisymmetric problems. Journal of Strain Analysis 22 (2), 115–126.

Endo, T., Oden, J.T., Becker, E.B., Miller, T., 1984. A numerical analysis of contact and limit-point behavior in a class of problems of finite elastic deformation. Computers and Structures 18, 899–910.

Feng, W.W., Huang, P., 1975. On the general contact problem of an inflated nonlinear plane membrane. International Journal of Solids and Structures 11, 437–448.

Humphrey, J.D., Strumpf, R.K., Yin, F.C.P., 1992. A constitutive theory for biomembranes: application to epicardium. ASME Journal of Biomechanical Engineering 114, 461–466.

Jenkins, C.H., Leonard, J.W., 1991. Nonlinear dynamic response of membranes: state of the art. Applied Mechanics Reviews 44, 319–328.

Kyriacou, S.K., Humphrey, J.D., 1996. Influence of size, shape and properties on the mechanics of axisymmetric saccular aneurysms. Journal of Biomechanics 29 (8), 1015–1022 (erratum 30: 761, 1997).

Ryan, J.M., Humphrey, J.D., 1999. Finite element based predictions of preferred material symmetries in saccular aneurysms. Annals of Biomedical Engineering 27, 641–647.

Sekhar, L.N., Heros, R.C., 1981. Origin, growth and rupture of saccular aneurysms: a review. Neurosurgery 8, 248–260.

Shah, A.D., Harris, J.L., Kyriacou, S.K., Humphrey, J.D., 1997. Further roles of geometry and properties in the mechanics of saccular aneurysms. Computational Methods in Biomechanics and Biomedical Engineering 1, 109–121.

Wiebers, D.O., et al., 1998. Unruptured intracranial aneurysms–risk of rupture and risks of surgical intervention. International study of unruptured intracranial aneurysm investigators. New England Journal of Medicine 339, 1725–1733.